Percutaneous Imaging-Guided Cryoablation of Liver Tumors: Predicting Local Progression on 24-Hour MRI

Paul B. Shyn[1]
Giovanni Mauri[1]
Raquel Oliva Alencar[1]
Servet Tatli[1]
Shaan H. Shah[1]
Paul R. Morrison[1,2]
Paul J. Catalano[3]
Stuart G. Silverman[1]

OBJECTIVE. The purpose of this study was to determine which MRI features observed 24 hours after technically successful percutaneous cryoablation of liver tumors predict subsequent local tumor progression and to describe the evolution of imaging findings after cryoablation.

MATERIALS AND METHODS. Thirty-nine adult patients underwent technically successful imaging-guided percutaneous cryoablation of 54 liver tumors (hepatocellular carcinoma, 8; metastases, 46). MRI features pertaining to the tumor, ablation margin, and surrounding liver 24 hours after treatment were assessed independently by two readers. Fisher exact or Wilcoxon rank sum tests (significant p values < 0.05) were used to compare imaging features in patients with and without subsequent local tumor progression. Imaging features of the ablation margin, treated tumor, and surrounding liver were evaluated on serial MRI in the following year.

RESULTS. A minimum ablation margin of 3 mm or less was observed in 11 (78.6%) of 14 tumors with and 15 of 40 (37.5%) without progression ($p = 0.012$). A blood vessel bridging the ablation margin was noted in 11 of 14 (78.6%) tumors with and nine of 40 (22.5%) without progression ($p < 0.001$). The incidence of tumor enhancement 24 hours after cryoablation was similar for tumors with (10/14, 71.4%) or without (25/40, 62.5%) local progression ($p = 0.75$). MRI enabled assessment of the entire cryoablation margin in 49 of 54 (90.7%) treated tumors.

CONCLUSION. MRI features at 24 hours after liver cryoablation that were predictive of local tumor progression included a minimum ablation margin less than or equal to 3 mm and a blood vessel bridging the ablation margin. Persistent tumor enhancement is common after liver cryoablation and does not predict local tumor progression.

Keywords: ablation procedures, cancer, gastrointestinal imaging, hepatobiliary system, MRI, vascular and interventional imaging

DOI:10.2214/AJR.13.10747

Received February 10, 2013; accepted after revision November 19, 2013.

[1]Division of Abdominal Imaging and Intervention, Department of Radiology, Brigham and Women's Hospital, Harvard Medical School, 75 Francis St, Boston, MA 02115. Address correspondence to P. B. Shyn (pshyn@partners.org).

[2]Deceased.

[3]Department of Biostatistics and Computational Biology, Dana-Farber Cancer Institute, Harvard Medical School, Boston, MA.

WEB
This is a web exclusive article.

AJR 2014; 203:W181–W191

0361–803X/14/2032–W181

Imaging-guided percutaneous thermal ablation techniques are minimally invasive nonsurgical alternative treatments for selected primary and metastatic hepatic malignancies [1–5]. Radiofrequency, microwave, and cryoablation are among the most common thermal ablation technologies used today [4, 6–9]. Liver cryoablation, in particular, had been used historically only during open surgery, largely because of the large size of the cryoprobes. Recently, renewed interest in hepatic cryoablation as a percutaneous technique has been facilitated by the development of smaller-diameter cryoprobes [10–13]. Percutaneous liver cryoablation is associated with lower complication rates compared with previously reported open cryosurgical series [14, 15]. The lower complication rates may be related to thinner cryoprobes and perhaps to reduced deforming forces on the frozen liver afforded by the closed percutaneous approach in comparison with the open surgical approach. Furthermore, percutaneous liver cryoablation offers advantages relative to other ablation technologies, including excellent ice ball visibility that facilitates precise control of the ablation zone relative to the tumor and critical structures. Finally, in our experience, the use of cryoablation to treat subcapsular liver tumors that require extension of the ablation zone into the adjacent diaphragm or body wall is associated with fewer complications and less postprocedural pain than radiofrequency ablation.

Imaging is essential in assessing the success of ablation procedures and in detecting local tumor progression early enough to enable prompt retreatment. Postablation imaging features have been well studied with respect to radiofrequency ablation [16–18].

However, the different mechanisms of inducing cellular death by cryoablation compared with radiofrequency ablation could lead to differences in observed postprocedure imaging features even though both mechanisms ultimately lead to tissue necrosis. Postablation imaging features used to predict local tumor progression are imperfect, in part because of limitations of imaging resolution and postablation changes in the margin [19].

MRI findings after liver tumor cryoablation have not been fully described with respect to expected postprocedure features or features predictive of local tumor progression [16–18, 20–22]. A recent report noted that residual liver tumor enhancement is common on MR images obtained after percutaneous cryoablation in patients without subsequent local tumor progression; however, it has not been established whether the presence or degree of enhancement differs between groups with and without local progression [21]. The objective of this study was to determine which MRI features observed 24 hours after technically successful percutaneous cryoablation of liver tumors predict subsequent local tumor progression and to describe the evolution of imaging findings after cryoablation.

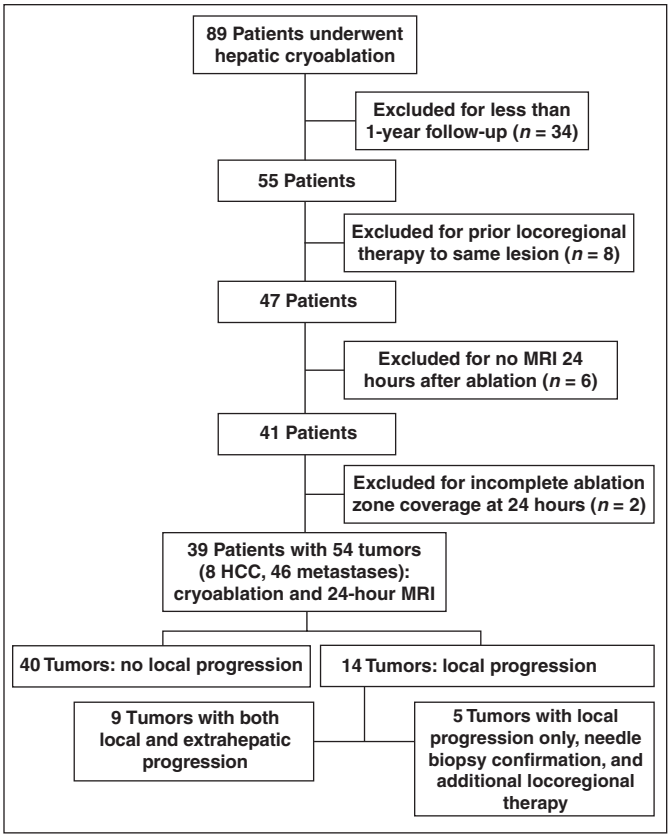

Fig. 1—Flowchart shows exclusion criteria resulting in final study population and subsequent groups of patients with and without local tumor progression HCC = hepatocellular carcinoma.

Materials and Methods

Patients and Procedures

This retrospective study was conducted with institutional review board approval and complied with HIPAA. The need for informed consent was waived. Our division's database of percutaneous imaging-guided tumor ablation procedures identified 89 patients who underwent cryoablation of liver tumors between 2005 and 2011. One year of imaging follow-up has been recommended as a minimum to exclude local tumor progression [23]. Thirty-four patients with insufficient imaging follow-up of less than 1 year were excluded. Other exclusion criteria included prior locoregional therapy to the ablated tumor, lack of 24-hour postablation imaging, and incomplete ablation zone coverage of the tumor at 24-hour MRI (Fig. 1).

Thirty-nine patients (23 men, 16 women; mean age, 52 years; range, 40–85 years) met the inclusion criteria. Nineteen of these patients were included in a previous study focused only on patients without local tumor progression [21]. Twenty-six patients had one tumor, 11 patients had two tumors, and two patients had three tumors treated. Accordingly, 54 liver tumors were analyzed and included hepatocellular carcinoma (n = 8), metastases from colorectal cancer (n = 11), gastrointestinal stromal tumor (n = 10), breast cancer (n = 6), ovarian cancer (n = 4), pancreatic neuroendocrine tumor (n = 4), esophageal cancer (n = 2), liposarcoma (n = 2), melanoma (n = 2), scalp angiosarcoma (n = 2), pancreatic adenocarcinoma (n = 1), tonsillar cancer (n = 1), and thymoma (n = 1). The largest diameters of the tumors ranged from 9 to 63 mm (mean, 30.3 mm; median, 30.0 mm). Tumors were located in Couinaud liver segments II (n = 2), III (n = 4), IVA (n = 4), IVB (n = 3), V (n = 9), VI (n = 10), VII (n = 9), and VIII (n = 13). Tumor cryoablation was performed using CT (n = 37) or MRI (n = 17) guidance. The procedures were performed with IV moderate sedation (n = 12) or general anesthesia (n = 27). One to seven (median, 4) 17-gauge cryoprobes were placed percutaneously for each treated tumor. The cryoprobes were connected to an argon-based cryoablation system (CryoHit, Galil Medical). The ablation protocol used a 15-minute freeze, 10-minute thaw (passive), and 15-minute freeze cycle.

MRI

MRI was performed with one of the following scanners: Signa Excite 1.5 T or HDx 3 T (GE Healthcare) or Magnetom Verio 3 T or Trio 3 T (Siemens Healthcare). Phased-array body coils were used. All examinations included unenhanced, breath-hold, 3D gradient-echo, and T1-weighted acquisitions. Fast spin-echo or turbo spin-echo T2-weighted sequences were also performed. T1-weighted dynamic contrast-enhanced acquisitions were performed in arterial, venous, late venous, and delayed phases. Gadopentetate dimeglumine (Magnevist, Bayer Healthcare) 0.1 mmol/kg (maximum, 10 mmol) was administered IV, followed immediately by a 10-mL saline flush. The arterial phase was defined by hepatic arterial enhancement without hepatic venous enhancement. Venous phase images showed initial enhancement of the hepatic veins. Late venous phase imaging followed the venous phase. The delayed phase was defined by imaging performed at 3 to 9 minutes after contrast material injection.

Image Analysis

Liver MRI examinations performed within 6 weeks before the cryoablation procedures were available to analyze for 42 of 54 tumors. MRI examinations were available to assess all 54 tumors at 24 hours, 35 tumors at 2–4 months, 29 tumors at 5–7 months, and 22 tumors at 8–12 months after cryoablation. Two board-certified radiologists with fellowship training in abdominal imaging and 5 and 21 years of experience after training independently reviewed all MRI examinations using a PACS workstation (Centricity, GE

Healthcare). Readers were blinded to all clinical information other than the fact that the patients had undergone percutaneous cryoablation of a liver tumor. Discrepancies were resolved by consensus review. Reviewers were aware of the timing of each scan in relation to the time of cryoablation and reviewed each patient's scans sequentially.

Initial Postcryoablation MRI

Table 1 lists MRI findings that were evaluated as potential predictors of local tumor progression at 24-hour postablation MRI. Visibility of the ablation margin was assessed on unenhanced T1-weighted, T2-weighted, and enhanced T1-weighted images [24]. The ablation margin was considered visible if the margin thickness separating underlying ablated tumor and overlying unablated normal liver could be measured circumferentially on all image slices through the ablation zone [23]. The MRI sequence that best showed the ablation margin was used for margin measurements. Maximum and minimum thicknesses of the ablation margin were measured [25]. For subcapsular tumors, the ablation margin was measured circumferentially even if it extended into adjacent perihepatic soft tissues (Fig. 2). In five of the 54 tumors in which the ablation margin was not visible in its entirety, the visible portions of the margins were used for measurements. No matter how wide the maximum or average ablation margin, the thinnest margin at any point along the circumference was reported as the minimum margin (Fig. 3). The presence of a bridging blood vessel at least 3 mm in diameter within the ablation margin contiguous with both underlying tumor and overlying unablated liver at a given point along the ablation margin was noted [26].

TABLE 1: MRI Variables at 24 Hours as Predictors of Subsequent Local Tumor Progression After Percutaneous Cryoablation of Liver Tumors

Variable	Ablated Tumors With Local Progression (*n* = 14)	Ablated Tumors Without Local Progression (*n* = 40)	*p*
Tumor T1 signal relative to normal liver			
Hyperintense	1 (7.1)	12 (30.0)	0.18
Hypointense	11 (78.6)	25 (62.5)	
Isointense	2 (14.3)	3 (7.5)	
Tumor T2 signal relative to normal liver			
Hyperintense	13 (92.9)	35 (87.5)	1.0
Hypointense	0 (0)	2 (5)	
Isointense	1 (7.1)	3 (7.5)	
Tumor enhancement present	10 (71.4)	25 (62.5)	0.75
Mean percentage tumor enhancement in peak phase	124.1 ± 90.1 (*n* = 10)	92.8 ± 63.0 (*n* = 25)	0.40
Ablation margin enhancement present	13 (92.9)	34 (85)	0.66
Periablational enhancement			
Transient vascular shunt	9 (64.3)	22 (55)	0.76
Arterial phase, thin rim	7 (50)	25 (62.5)	0.53
Venous phase, thin rim	9 (64.3)	24 (60)	1.000
Venous phase, thick rim	2 (14.1)	6 (15)	1.000
Blood vessel bridging ablation margin	11 (78.6)	9 (22.5)	< 0.001[a]
Minimum margin ≤ 3 mm	11 (78.6)	15 (37.5)	0.012[a]
Mean minimum ablation margin (mm)	1.9 ± 3.2	4.9 ± 3.1	0.004[a]

Note—Data are number with percentage in parentheses or mean ± SD.
[a]Statistically significant.

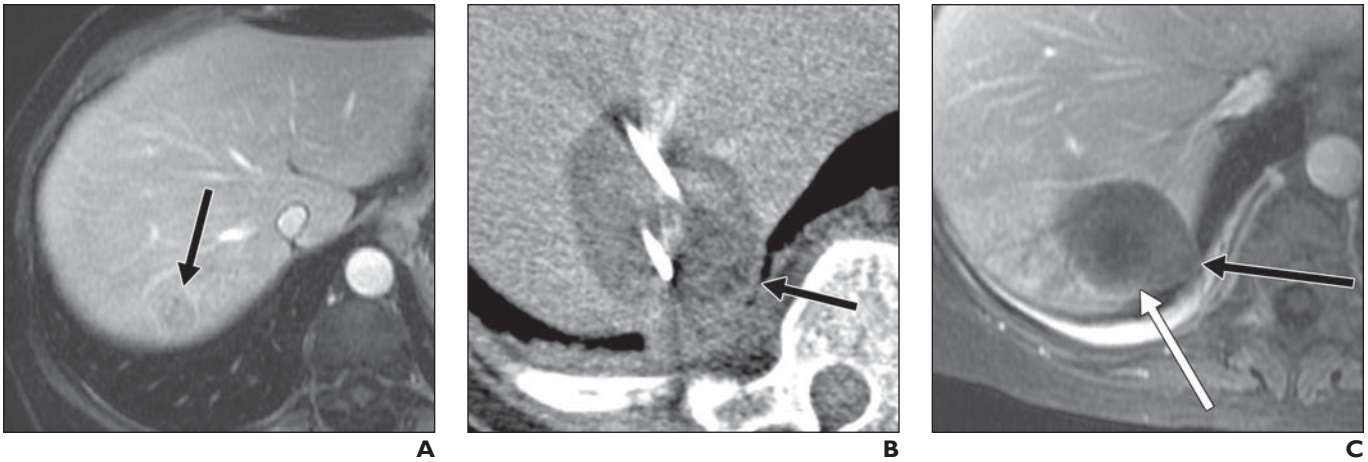

Fig. 2—48-year-old woman with solitary liver metastasis from breast cancer.
A, Contrast-enhanced T1-weighted MRI shows 2.5-cm subcapsular tumor (*arrow*).
B, CT image obtained during cryoablation depicts hypodense ice ball extending through diaphragm and slightly into adjacent lung parenchyma (*arrow*).
C, Contrast-enhanced T1-weighted MRI obtained 24 hours after cryoablation shows hypointense ablation zone and ablation margin not only in liver but also extending beyond liver and diaphragm (*black arrow*). This tumor was one of five study tumors in which ablation margin was not distinctly visible at all points along tumor circumference (*white arrow*). Nevertheless, no local progression was observed through 46 months of imaging follow-up in this patient.

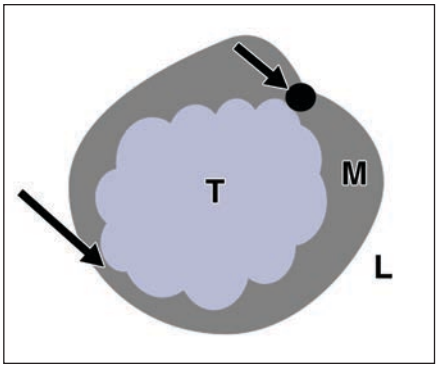

Fig. 3—Drawing shows diagram of ablation zone. Long arrow indicates minimum ablation margin thickness, and short arrow indicates blood vessel (≥ 3 mm) bridging ablation margin and contiguous with both tumor and unablated liver at single point along margin circumference. T = ablated tumor, M = ablation margin, L = unablated liver. (Drawing by Shyn PB)

The subjective predominant signal intensity (SI) of each tumor and the ablation margin on unenhanced T1-weighted and T2-weighted images were noted as hypo-, iso-, or hyperintense relative to normal liver parenchyma [23]. Objective assessment of contrast enhancement was obtained by recording region of interest SI measurements of the ablated tumor, the ablation margin, the periablational liver, and normal liver. SI measurements were obtained from each phase of the dynamic acquisition and compared with unenhanced measurements. Percentage enhancement was calculated using the formula [(*SI enhanced* − *SI unenhanced*) / *SI unenhanced*] × 100. Tumor SI was measured in the visually most enhancing region of the tumor on the phase showing peak enhancement and using the same region for all other phases. A 15% threshold was used to confirm enhancement on the peak tumor enhancement phase [27]. The pattern of tumor enhancement, when it reached this threshold, was assigned one of four possible patterns previously encountered in our practice: homogeneous, inhomogeneous, thin rim, or thick rim (> 2.5 mm). For enhancing tumors, progressive centripetal enhancement was noted if present. Periablational enhancement, if present, was classified into one of the following patterns: transient arterial phase thin rim enhancement, transient arterial phase shunt (usually wedge-shaped or polygonal), and thin or thick (> 3 mm) rim hyperemia in the venous or later phase [19].

Evaluation of Evolution of MRI Findings

MRI features assessed on the 24-hour study were also assessed on studies at all other available time points (Table 2). In addition, the long (*D1*) and perpendicular (*D2*) short-axis diameters of the ablation zone were measured on each MRI examination, and the maximum cross-sectional area of the ablation zone was calculated, assuming an ellipse (π /4 × *D1* × *D2*). Percentage changes in cross-sectional area of the ablation zone were calculated at each subsequent time point relative to the 24-hour measurement. Features suggestive of a fibrous capsule, including T1 and T2 hypointensity as well as late enhancement, were noted when present within the periphery of the ablation zone.

Determination of Tumor Recurrence and Progression

The mean duration of imaging follow-up using CT, MRI, or PET/CT was 30.3 months (range, 13–72 months). Progression of imaging findings on follow-up CT, MRI, or PET/CT was used to assess local tumor recurrence and progression at the site of cryoablation. For CT or MRI studies obtained after the 24-hour postablation MRI, any new enhancing nodule or eccentric thickening within or contiguous with the ablation zone and any ablation zone enlargement were considered suspicious for local tumor progression [19, 23, 26]. Any new focal ^{18}F-FDG uptake on PET/CT within or adjacent to the ablation margin was considered suspicious also [28]. Suspicious findings were then correlated with all subsequent imaging. Biopsy was not performed in patients with imaging findings of both hepatic and extrahepatic progression that precluded further local therapies. Absence of local progression was defined as a stable or reduced size of the cryoablation zone compared with the 24-hour MRI examination and absence of the suspicious imaging findings described in this paragraph on the basis of imaging follow-up of at least 1 year [23]. Biopsy was not required to confirm the absence of local tumor progression; biopsy procedures were not indicated clinically.

Statistical Analysis

The mean minimum ablation margin thickness and the mean peak percentage tumor enhancement on 24-hour MRI were compared between groups with and without subsequent local tumor progression using the Wilcoxon rank sum test. All other MRI features were compared using the Fisher exact test. All statistical tests were two-sided; *p* values less than 0.05 were considered significant. The evolution of imaging findings up to 1 year after cryoablation are described in Table 2 for all study tumors as the percentage of tumors showing the finding at each time-point. The dynamic MRI contrast enhancement patterns of all study tumors, ablation margins, periablational zones, and normal liver were depicted graphically as mean percentage enhancement values from MRI examinations obtained before and up to 1 year after cryoablation (Fig. 4).

Results

Overall, local tumor progression occurred in 14 of 54 (26%) cryoablated tumors. Local progression did not occur in 40 of 54 (74%) cryoablated liver tumors. Five tumors (in five patients) had only intrahepatic local progression and underwent subsequent local therapy, including percutaneous cryoablation of four recurrences and radiofrequency ablation of one. Fine-needle aspiration biopsy confirmed local progression for each of these five tumors. Nine patients had both intrahepatic local tumor progression at the cryoablation site and extrahepatic progression of tumor, which precluded further local therapies.

The ablation margin was distinct from ablated tumor and surrounding unablated liver at 24 hours on at least one MRI sequence, enabling assessment of the entire cryoablation margin in 49 of 54 (90.7%) tumors. Visibility of the entire ablation margin was most reliably detected on dynamic contrast-enhanced images and often visible on T2-weighted and unenhanced T1-weighted images (Table 2).

Regarding the use of MRI features to predict local progression, the mean minimum ablation margin was 1.9 ± 3.2 mm in ablated tumors with subsequent local progression and 4.9 ± 3.1 mm in those without local progression (p = 0.004) (Table 1). Local tumor progression developed in 11 of 26 (42.3%) tumors with a minimum ablation margin less than or equal to 3 mm but only developed in three of 28 (10.7%) tumors with a minimum margin greater than 3 mm (p = 0.012). The odds ratio for progression with a margin less than or equal to 3 mm compared with greater than 3 mm was 6.11 (95% CI,1.28–38.26). A 5-mm threshold for local progression did not achieve statistical significance, however, only two tumors with a minimum margin greater than 5 mm showed local progression. Local progression developed in 11 of 20 (55.0%) tumors with a blood vessel (≥ 3 mm) bridging the ablation margin but only developed in three of 34 (8.8%) tumors without a bridging vessel (p < 0.001) (Fig. 5). The odds ratio for progression with presence compared with absence of a bridging blood vessel was 12.63 (2.46–81.00). No other 24-hour MRI feature correlated with subsequent local tumor progression. Specifically, 41 of 42 (97.6%) tumors showed contrast

TABLE 2: Evolution of MRI Features Up to 1 Year After Percutaneous Cryoablation of Liver Tumors With or Without Local Tumor Progression

	Time Point of MRI Relative to Cryoablation (Total No. of Tumors Evaluated)				
	Before (*n* = 42)	24 h (*n* = 54)	2–4 mo (*n* = 35)	5–7 mo (*n* = 29)	8–12 mo (*n* = 22)
Tumor, T1 signal intensity relative to normal liver					
Hyperintense	6 (14.3)	13 (24.1)	13 (37.1)	9 (31.0)	7 (31.8)
Hypointense	34 (81.0)	36 (66.7)	14 (40)	10 (34.5)	8 (36.4)
Isointense	2 (4.8)	5 (9.3)	8 (22.9)	10 (34.5)	7 (31.8)
Tumor, T2 signal intensity relative to normal liver					
Hyperintense	36 (85.7)	48 (88.9)	21 (60.0)	11 (37.9)	7 (31.8)
Hypointense	3 (7.1)	2 (3.7)	9 (25.7)	9 (31.0)	7 (31.8)
Isointense	3 (7.1)	4 (7.4)	5 (14.3)	9 (31.0)	8 (36.4)
Ablation margin, T1 signal intensity relative to normal liver					
Hyperintense	NA	1 (1.9)	20 (57.1)	8 (27.6)	6 (27.3)
Hypointense	NA	53 (98.1)	9 (25.7)	15 (51.7)	8 (36.4)
Isointense	NA	0 (0.0)	6 (17.1)	6 (20.7)	8 (36.4)
Ablation margin, T2 signal intensity relative to normal liver					
Hyperintense	NA	11 (20.4)	13 (37.1)	18 (62.1)	12 (54.5)
Hypointense	NA	36 (66.7)	16 (45.7)	8 (27.6)	6 (27.3)
Isointense	NA	7 (13.0)	6 (17.1)	3 (10.3)	4 (18.2)
Ablation margin, visually distinct from tumor and normal liver (more than one sequence may be positive)					
T1-weighted imaging	NA	33 (61.1)	21 (60.0)	11 (37.9)	8 (36.4)
T2-weighted imaging	NA	39 (72.2)	15 (42.9)	12 (41.4)	5 (22.7)
T1 dynamic contrast-enhanced imaging	NA	43 (79.6)	14 (40.0)	13 (44.8)	8 (36.4)
Tumor, no. with enhancement	*n* = 41 (97.6)	*n* = 35 (64.8)	*n* = 13 (37.1)	*n* = 11 (37.9)	*n* = 7 (31.8)
Pattern of tumor enhancement (more than one pattern possible)					
Homogeneous	2 (4.9)	2 (5.7)	0 (0.0)	0 (0.0)	2 (28.6)
Inhomogeneous	18 (43.9)	12 (34.3)	5 (38.5)	2 (18.2)	2 (28.6)
Thin rim	5 (12.2)	8 (22.9)	2 (15.4)	3 (27.3)	1 (14.3)
Thick rim	16 (39.0)	13 (37.1)	6 (46.2)	6 (54.5)	2 (28.6)
Centripetal filling	NA	9 (25.7)	1 (7.7)	1 (9.1)	1 (14.3)
Phase of peak tumor enhancement					
Arterial	2 (4.9)	0 (0.0)	0 (0.0)	0 (0.0)	0 (0.0)
Venous	16 (39.0)	7 (20.0)	3 (23.1)	1 (9.1)	0 (0.0)
Late venous	15 (36.6)	12 (34.3)	3 (23.1)	3 (27.3)	2 (28.6)
Delayed	8 (19.5)	16 (45.7)	7 (53.9)	7 (63.6)	5 (71.4)
Ablation margin, no. with enhancement	*n* = 41 (97.6)	*n* = 47 (87.0)	*n* = 25 (71.4)	*n* = 20 (69.0)	*n* = 19 (86.4)
Phase of peak enhancement					
Arterial	2 (4.9)	0 (0.0)	2 (8.0)	0 (0.0)	0 (0.0)
Venous	30 (73.2)	6 (12.8)	4 (16.0)	1 (5.0)	0 (0.0)
Late venous	9 (22.0)	9 (19.1)	2 (8.0)	3 (15.0)	3 (15.8)
Delayed	0 (0.0)	32 (68.1)	17 (68.0)	16 (80.0)	16 (84.2)

(Table 2 continues on next page)

TABLE 2: Evolution of MRI Features Up to 1 Year After Percutaneous Cryoablation of Liver Tumors With or Without Local Tumor Progression (continued)

	Time Point of MRI Relative to Cryoablation (Total No. of Tumors Evaluated)				
	Before (n = 42)	24 h (n = 54)	2–4 mo (n = 35)	5–7 mo (n = 29)	8–12 mo (n = 22)
Periablational liver, phase of peak enhancement					
Arterial	NA	10 (18.5)	3 (8.6)	3 (10.3)	1 (4.5)
Venous	NA	31 (57.4)	16 (45.7)	16 (55.2)	7 (31.8)
Late venous	NA	12 (22.2)	14 (40)	9 (31.0)	10 (45.5)
Delayed	NA	1 (1.9)	2 (5.7)	1 (3.4)	4 (18.2)
Periablational enhancement pattern during arterial phase					
Thin rim	NA	12 (22.2)	3 (8.6)	3 (10.3)	3 (13.6)
Shunt	NA	11 (20.4)	11 (31.4)	9 (31.0)	3 (13.6)
Both	NA	20 (37.0)	5 (14.3)	1 (3.4)	0 (0.0)
None	NA	11 (20.4)	16 (45.7)	16 (55.2)	16 (72.7)
Periablational enhancement pattern during venous or later phases					
Thin rim	NA	33 (61.1)	11 (31.4)	8 (27.6)	8 (36.4)
Thick rim	NA	8 (14.8)	8 (22.9)	8 (27.6)	3 (13.6)
None	NA	13 (24.1)	16 (45.7)	13 (44.8)	11 (50.0)
Normal liver, phase of peak enhancement					
Arterial	0 (0.0)	2 (3.7)	1 (2.9)	0 (0.0)	0 (0.0)
Venous	29 (69.0)	35 (64.8)	24 (68.6)	21 (72.4)	15 (68.2)
Late venous	13 (31.0)	15 (27.8)	9 (25.7)	8 (27.6)	7 (31.8)
Delayed	0 (0.0)	2 (3.7)	1 (2.9)	0 (0.0)	0 (0.0)
Fibrous capsule present	NA	0 (0.0)	18 (51.4)	15 (51.7)	14 (63.6)
Mean percentage decrease in ablation zone area compared with 24 h (mm^2)	NA	NA	55.6 ± 15.6	68.3 ± 12.5	63.9 ± 13.1

Note— Data are number with percentage in parentheses or mean ± SD.. The number of tumor regions evaluated for each category of MRI findings is the same as the total number of tumors evaluated at each time point unless otherwise specified. NA = not applicable.

enhancement before cryoablation, and 35 of 54 (64.8%) showed enhancement 24 hours after cryoablation. The incidence of tumor enhancement at 24 hours was not significantly different between tumors with or without subsequent local progression ($p = 0.75$). Persistent enhancement was even more common in the ablation margin than in the cryoablated tumor and also did not correlate with subsequent local tumor progression ($p = 0.66$).

The evolution of MRI features over time is detailed in Table 2. Among these, most cryoablated tumors, irrespective of eventual local tumor progression, were hypointense on T1-weighted images and hyperintense on T2-weighted images at 24 hours but became more variable in relative SI at later time points. The ablation margin was almost always hypointense on T1-weighted images and usually hypointense on T2-weighted images at 24 hours, also becoming more variable at later time points (Fig. 6). The ablation margin became progressively more difficult to visualize at each successive time-point beyond 24 hours.

Tumor enhancement decreased over time but persisted in seven of 22 (31.8%) tumors at 8–12 months, and only two of these seven tumors were associated with local progression. The mean peak percentage enhancement of tumors decreased most prominently 24 hours after cryoablation and continued to decrease thereafter (Fig. 4). A shift in the phase of peak tumor enhancement from arterial or venous phases before cryoablation to late venous or delayed phases after cryoablation was observed and became more pronounced at each successive follow-up time-point. A similar shift in peak enhancement phase of the ablation margin to later phases was observed following cryoablation. The mean ablation zone area decreased by 55.6% ± 15.6 at 2–4 months and 63.9% ± 13.1 at 8–12 months. Imaging findings suggestive of a fibrous capsule were observed in 18 of 35 (51.4%) tumors imaged at 3 months after cryoablation, increasing to 14 of 22 (63.6%) at 8–12 months (Fig. 7).

Discussion

Contrast-enhanced MRI is routinely performed 24 hours after percutaneous liver tumor cryoablation and before discharge at our institution [29]. MRI is used to exclude complications, provide immediate assessment of results, and provide a baseline for future comparisons. Imaging features in this study predictive of subsequent local tumor progression were presence of a blood vessel (≥ 3 mm) bridging the ablation margin or a small (≤ 3 mm) minimum ablation margin. Only two of 54 cryoablated tumors with a minimum ablation margin larger than 5 mm developed subsequent local progression. Therefore, a minimum ablation margin exceeding 5 mm is recommended.

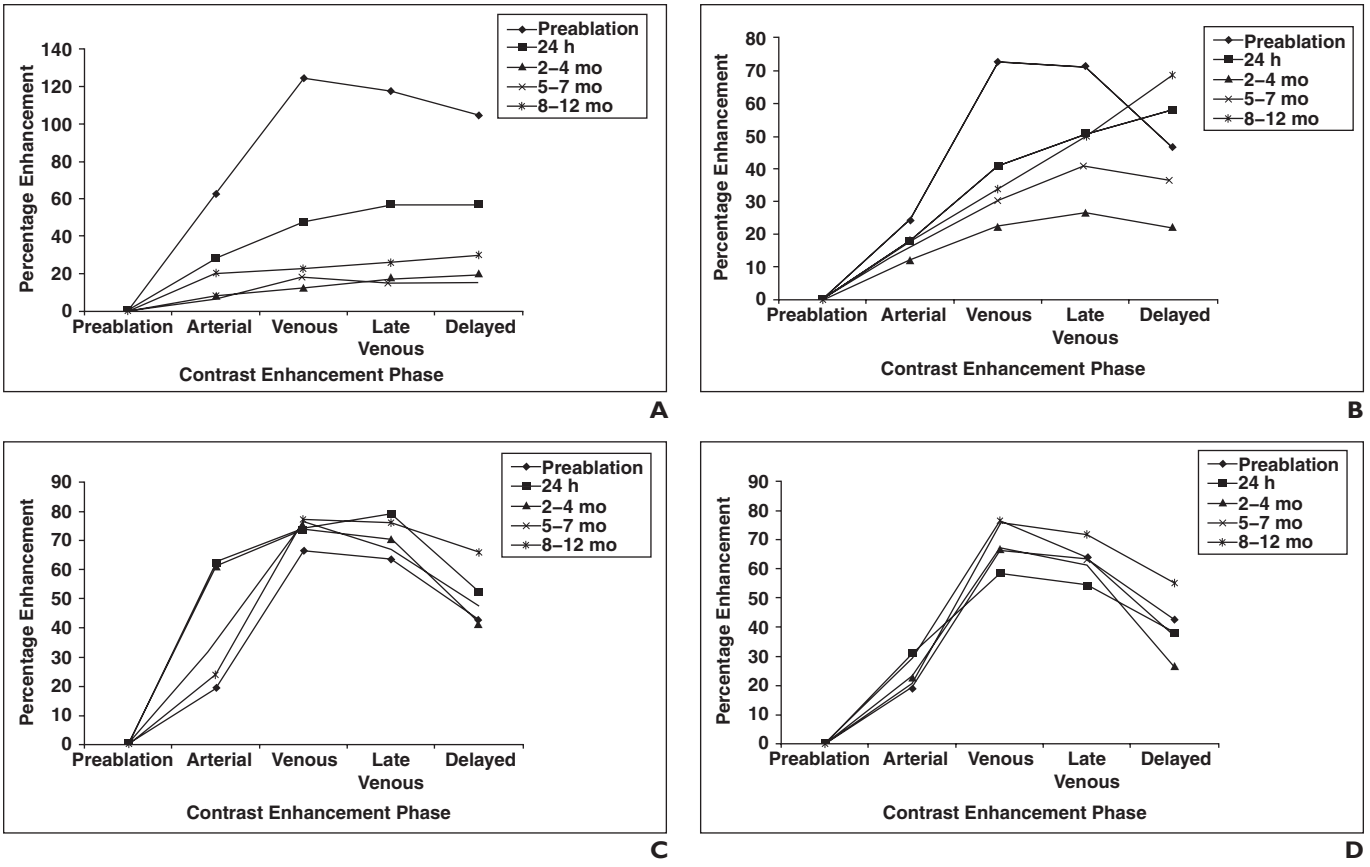

Fig. 4—Mean percentage contrast enhancement on basis of region-of-interest measurements in all 54 cryoablated tumors
A–D, Graphs show tumor (**A**), ablation margins (**B**), periablational zones (**C**), and normal liver parenchyma (**D**) on dynamic contrast-enhanced MRI before ablation and at four time points after ablation.

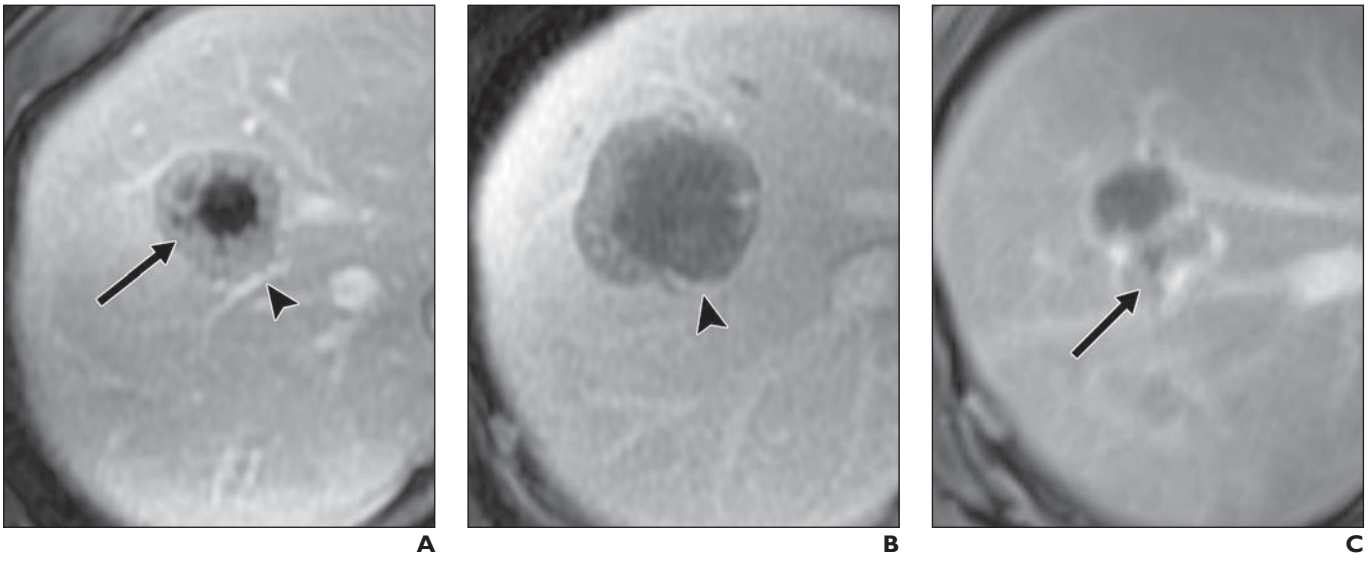

Fig. 5—47-year-old man with liver metastasis from tonsillar carcinoma.
A, Preprocedure contrast-enhanced T1-weighted image shows centrally necrotic metastasis (*arrow*) in segment VIII with multiple contiguous blood vessels, including one (*arrowhead*) at 5-o'clock position.
B, Contrast-enhanced T1-weighted MRI obtained 24 hours after cryoablation shows blood vessel or heat sink (*arrowhead*) contiguous with both underlying tumor (markedly hypointense) and overlying unablated liver in thinnest (2 mm) region of ablation margin (mildly hypointense).
C, Contrast-enhanced MRI obtained 5 months later reveals new peripheral nodular enhancement (*arrow*) in same location, consistent with local tumor progression.

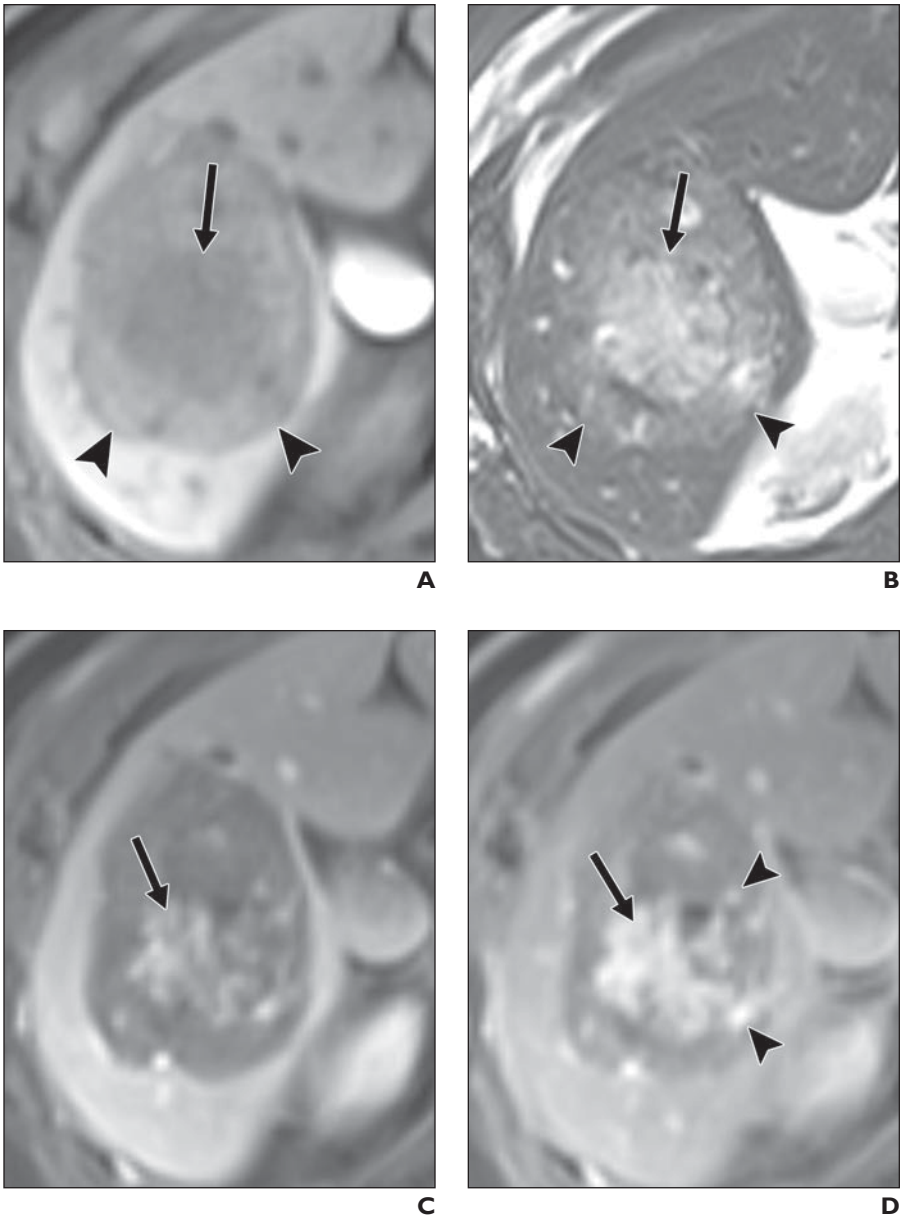

Fig. 6—40-year-old woman with breast carcinoma who underwent percutaneous cryoablation of liver metastasis.
A, Unenhanced T1-weighted MRI obtained 24 hours after cryoablation depicts interface (*arrow*) of hypointense ablation margin with very hypointense ablated tumor and interface (*arrowheads*) of ablation margin with adjacent unablated liver.
B, T2-weighted image also shows entire circumference of ablation margin including tumor interface (*arrow*) and unablated liver interface (*arrowheads*). Tumor is hyperintense. Minimum ablation margin thickness was 5 mm, and no recurrence was observed during 23 months of imaging follow-up.
C and **D,** Venous phase (**C**) and delayed phase (**D**) images show tumor enhancement (*arrow*) that progressively increases in delayed phase image. Note reperfused vessels (*arrowheads*, **D**) coursing through ablation margin and tumor.

Understanding which two liver MRI features are predictive of local tumor progression may help radiologists interpret MRI examinations after percutaneous liver ablations and ultimately identify at an early stage which patients need additional treatment or closer surveillance.

Cryoablation freezes tissues to temperatures less than –20° to –30°C and causes tissue necrosis through mechanisms different from radiofrequency ablation [30]. Direct injury to cell membranes results from intracellular and extracellular ice formation accentuated by repeated freeze-thaw cycles. Indirect cellular damage results from disruption of the vascular endothelium that accentuates thrombosis or reperfusion injury [31–34]. This study shows that the cryoablated tumor "ghost" is often well visualized on MRI, enabling delineation of the ablation margin on at least one or more MRI sequences. The ablation margin represents the rim of normal liver surrounding the ablated tumor and included in the ablation zone to ensure complete destruction of potential adjacent microscopic tumor.

Radiofrequency ablation is the most widely used liver ablation technology and causes tumor coagulation by heating tissues to temperatures of at least 50–60°C [30]. After radiofrequency ablation, absence of enhancement in completely treated tumors is expected, whereas persistent or new enhancement suggests incomplete treatment [16–18, 20, 35, 36]. The ablation margin is often estimated on MRI or CT images after radiofrequency ablation procedures by comparing the original tumor size and shape with the hypoenhancing ablation zone. Because radiofrequency ablated tumors are indistinct or not visible in 37–71% of ablation zones, it is difficult to identify and accurately report the true minimum ablation margin [37, 38]. This problem has prompted studies using registration techniques of pre- and postablation imaging to improve assessment of the ablation margin [39, 40]. In contradistinction, 24-hour MRI after liver cryoablation appeared to enable complete assessment of the ablation margin in 49 of 54 (90.7%) tumors in this study, enabling the minimum ablation margins to be reported. The dynamic contrast-enhanced T1-weighted acquisition was the most reliable sequence for visualizing the ablation margin, although differences in T1 or T2 SI on unenhanced acquisitions were also helpful (Table 2). The ablation margin typically enhanced less than surrounding unablated liver tissue, particularly in the arterial and venous phases (Fig. 6). In late venous and delayed phases, enhancement of the margin tended to increase as enhancement in the unablated liver decreased, sometimes resulting in decreased conspicuity of the margin. Visibility of the ablation margin progressively decreased on follow-up MRI.

We previously reported that persistent liver tumor enhancement is common after cryoablation in patients without subsequent local tumor progression, and similar findings have

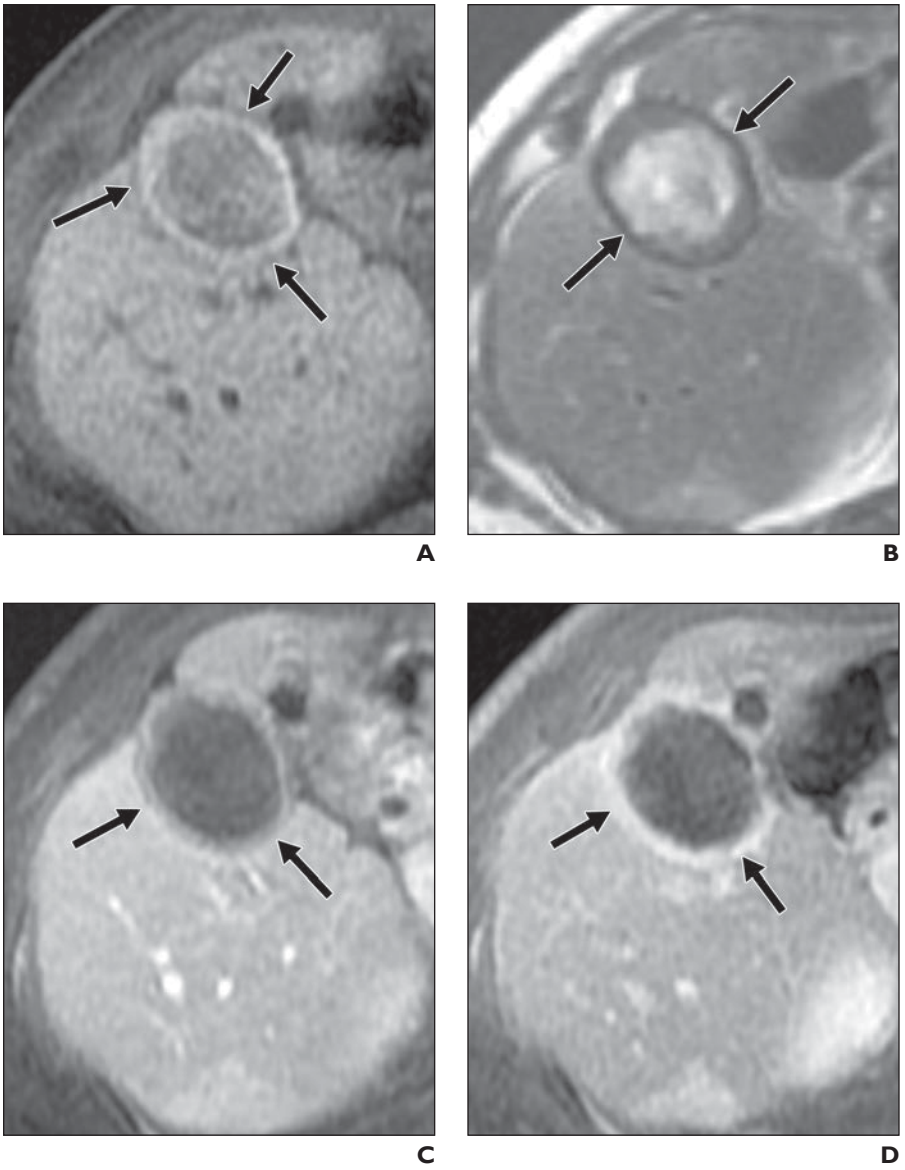

Fig. 7—45-year-old woman 3 months after cryoablation of liver metastasis from gastrointestinal stromal tumor.
A, Unenhanced T1-weighted MRI of fibrous capsule (*arrows*) defines outermost extent of cryoablation margin and is hypointense.
B, Capsule (*arrows*) is hypointense on T2-weighted image.
C and **D,** Minimal capsular enhancement (*arrows*) is apparent on venous phase image (**C**) but prominent enhancement (*arrows*) is observed on delayed phase image (**D**).

been described by others after renal tumor cryoablation [21, 41]. This study establishes that persistent enhancement of the tumor and ablation margin after liver cryoablation is common and not statistically different between patients with or without subsequent local tumor progression. The percentage tumor enhancement was also not significantly different between groups. Persistent tumor and ablation margin enhancement sometimes included reperfused blood vessels that coursed into and out of the ablation zone. Freeze injury of blood vessels may lead to vasodilation and leakiness, which, along with reperfusion, may account for the observed contrast-enhancement findings. For example, tumor enhancement after cryoablation tended to peak in later dynamic phases than was observed before cryoablation. Reperfusion of the cryoablation zone also explains the occasional observation of centripetal enhancement of the cryoablation zone on dynamic acquisitions. Persistent tumor or ablation margin enhancement that occurred in the absence of local tumor progression was invariably present at 24 hours and did not initially appear on subsequent follow-up MRI.

The cryoablation zone involuted rapidly over time, with a mean decrease of 55.6% in cross-sectional area at 2–4 months. The involution often appeared proportionately greater in the ablation margin than in the ablated tumor, although this was not quantified. Accordingly, the ablation margin is ideally evaluated on 24-hour MRI because subsequent involution makes assessment of the margin progressively more difficult. Enhancement in the rim of liver surrounding the ablation zone, referred to as "benign periablational enhancement," was commonly seen after cryoablation, as it is after radiofrequency ablation, either as a thin rim of hyperemia in the arterial phase or as a thick halo in the venous phase [42]. As with radiofrequency ablation, arterial phase transient shunt enhancement was also often noted around cryoablation zones.

We occasionally observed a peripheral ring of enhancement within the ablation margin that might simulate benign periablational enhancement. Periablational enhancement, however, occurs in the unablated liver tissue immediately peripheral to the ablation margin (Fig. 3). As early as 3 months after cryoablation, a rim of enhancement can be seen that suggests a developing fibrous capsule defining the outer limits of the cryoablation zone. The presumed fibrous capsule develops within the peripheral part of the ablation margin. The key features suggesting a fibrous capsule were T1 and T2 hypointensity and contrast enhancement that first appeared or persisted on delayed phases (Fig. 7). Periablational enhancement, on the other hand, corresponded to viable tissue that was not T1 and T2 hypointense and enhanced early or transiently. Distinguishing a fibrous capsule from periablational enhancement is likely to be important in defining the actual boundary of the ablation zone. The fibrous capsule may further prove useful in that we have not observed tumor recurring in or inside of a fibrous capsule.

The retrospective nature of this study imposed certain limitations, including the use of multiple MRI scanners and sequence parameters that could have affected the imaging findings. Diffusion-weighted imaging was not routinely performed during the study period and therefore is not included

in this analysis. Some patients did not undergo follow-up MRI studies at each time point beyond the initial 24-hour postprocedure study, and that limited the analysis of time-points beyond 24 hours. MRI findings at 8–12 months could potentially have been affected by repeat ablation procedures of three study tumors. Dynamic or temporal changes in contrast enhancement were not analyzed as predictors of local progression. Results were not analyzed by histologic tumor subtype because a much larger study would be required to yield statistically significant data. The absence of local tumor progression was established on the basis of at least 1 year of imaging follow-up, and pathology (biopsy or surgical resection) could not be justified clinically in these patients. Additionally, follow-up imaging modalities used to confirm progression or lack of progression included CT, MRI, or PET/CT in various combinations because of the retrospective nature of this study. The MRI assessment of the ablation margin relied on SI differences between ablated tumor, the ablation margin, and surrounding unablated liver; however, histopathologic confirmation of the imaging assessment of the ablation margin was not possible. Finally, it should be emphasized that our study was not intended to compare the performance of liver cryoablation with other ablation technologies. Rather, our study results may assist radiologists who perform liver cryoablation procedures or who interpret the follow-up imaging studies used to guide subsequent patient care.

In conclusion, liver tumor enhancement on MRI after percutaneous cryoablation is common and alone does not indicate inadequate treatment; however, a small (≤ 3 mm) minimum ablation margin or the presence of a blood vessel (≥ 3 mm) bridging the ablation margin are each predictive of local progression.

References

1. Lencioni R, Crocetti L. Local-regional treatment of hepatocellular carcinoma. *Radiology* 2012; 262:43–58
2. Solbiati L, Ahmed M, Cova L, Ierace T, Brioschi M, Goldberg SN. Small liver colorectal metastases treated with percutaneous radiofrequency ablation: local response rate and long-term survival with up to 10-year follow-up. *Radiology* 2012; 265:958–968
3. Otto G, Düber C, Hoppe-Lotichius M, König J, Heise M, Pitton MB. Radiofrequency ablation as first-line treatment in patients with early colorectal liver metastases amenable to surgery. *Ann Surg* 2010; 251:796–803
4. Solbiati L, Livraghi T, Goldberg SN, et al. Percutaneous radio-frequency ablation of hepatic metastases from colorectal cancer: long-term results in 117 patients. *Radiology* 2001; 221:159–166
5. Tiong L, Maddern GJ. Systematic review and meta-analysis of survival and disease recurrence after radiofrequency ablation for hepatocellular carcinoma. *Br J Surg* 2011; 98:1210–1224
6. Pacella CM, Francica G, Di Lascio FM, et al. Long-term outcome of cirrhotic patients with early hepatocellular carcinoma treated with ultrasound-guided percutaneous laser ablation: a retrospective analysis. *J Clin Oncol* 2009; 27:2615–2621
7. Veltri A, Gazzera C, Rotondella C, Camerano F, Busso M, Gandini G. Image-guided microwave ablation of hepatic tumours: preliminary experience. *Radiol Med (Torino)* 2012; 117:378–392
8. Livraghi T, Meloni F, Solbiati L, Zanus G. Complications of microwave ablation for liver tumors: results of a multicenter study. *Cardiovasc Intervent Radiol* 2012; 35:868–874
9. Morrison PR, Silverman SG, Tuncali K, Tatli S. MRI-guided cryotherapy. *J Magn Reson Imaging* 2008; 27:410–420
10. Silverman SG, Sun MR, Tuncali K, et al. Three-dimensional assessment of MRI-guided percutaneous cryotherapy of liver metastases. *AJR* 2004; 183:707–712
11. Hinshaw JL, Lee FT. Cryoablation for liver cancer. *Tech Vasc Interv Radiol* 2007; 10:47–57
12. Silverman SG, Tuncali K, Adams DF, et al. MR imaging-guided percutaneous cryotherapy of liver tumors: initial experience. *Radiology* 2000; 217:657–664
13. Bang HJ, Littrup PJ, Currier BP, et al. Percutaneous cryoablation of metastatic lesions from non-small-cell lung carcinoma: initial survival, local control, and cost observations. *J Vasc Interv Radiol* 2012; 23:761–769
14. Pearson AS, Izzo F, Fleming RY, et al. Intraoperative radiofrequency ablation or cryoablation for hepatic malignancies. *Am J Surg* 1999; 178:592–599
15. Seifert JK, Morris DL. World survey on the complications of hepatic and prostate cryotherapy. *World J Surg* 1999; 23:109–113
16. Crocetti L, Della Pina C, Cioni D, Lencioni R. Peri-intraprocedural imaging: US, CT, and MRI. *Abdom Imaging* 2011; 36:648–660
17. Vossen JA, Buijs M, Kamel IR. Assessment of tumor response on MR imaging after locoregional therapy. *Tech Vasc Interv Radiol* 2006; 9:125–132
18. Kierans AS, Elazzazi M, Braga L, et al. Thermoablative treatments for malignant liver lesions: 10-year experience of MRI appearances of treatment response. *AJR* 2010; 194:523–529
19. Goldberg SN, Grassi CJ, Cardella JF, et al. Image-guided tumor ablation: standardization of terminology and reporting criteria. *Radiology* 2005; 235:728–739
20. Park MH, Rhim H, Kim YS, Choi D, Lim HK, Lee WJ. Spectrum of CT findings after radiofrequency ablation of hepatic tumors. *RadioGraphics* 2008; 28:379–390
21. Shyn PB, Oliva MR, Shah SH, Tatli S, Catalano PJ, Silverman SG. MRI contrast enhancement of malignant liver tumours following successful cryoablation. *Eur Radiol* 2012; 22:398–403
22. Limanond P, Zimmerman P, Raman SS, Kadell BM, Lu DS. Interpretation of CT and MRI after radiofrequency ablation of hepatic malignancies. *AJR* 2003; 181:1635–1640
23. Gervais DA, Kalva S, Thabet A. Percutaneous image-guided therapy of intra-abdominal malignancy: imaging evaluation of treatment response. *Abdom Imaging* 2009; 34:593–609
24. Koda M, Tokunaga S, Miyoshi K, et al. Assessment of ablative margin by unenhanced magnetic resonance imaging after radiofrequency ablation for hepatocellular carcinoma. *Eur J Radiol* 2012; 81:2730–2736
25. Wang X, Sofocleous CT, Erinjeri JP, et al. Margin size is an independent predictor of local tumor progression after ablation of colon cancer liver metastases. *Cardiovasc Intervent Radiol* 2013; 36:166–175
26. Kim YS, Rhim H, Cho OK, Koh BH, Kim Y. Intrahepatic recurrence after percutaneous radiofrequency ablation of hepatocellular carcinoma: analysis of the pattern and risk factors. *Eur J Radiol* 2006; 59:432–441
27. Ho VB, Allen SF, Hood MN, Choyke PL. Renal masses: quantitative assessment of enhancement with dynamic MR imaging. *Radiology* 2002; 224:695–700
28. Chen W, Zhuang H, Cheng G, Torigian DA, Alavi A. Comparison of FDG-PET, MRI and CT for post radiofrequency ablation evaluation of hepatic tumors. *Ann Nucl Med* 2013; 27:58–64
29. Nair RT, Silverman SG, Tuncali K, Obuchowski NA, vanSonnenberg E, Shankar S. Biochemical and hematologic alterations following percutaneous cryoablation of liver tumors: experience in 48 procedures. *Radiology* 2008; 248:303–311
30. Ahmed M, Brace CL, Lee FT, Goldberg SN. Principles of and advances in percutaneous ablation. *Radiology* 2011; 258:351–369
31. Gage AA, Baust J. Mechanisms of tissue injury in cryosurgery. *Cryobiology* 1998; 37:171–186
32. Mazur P. Freezing of living cells: mechanisms and implications. *Am J Physiol* 1984; 247:C125–C142
33. Jansen MC, van Hillegersberg R, Schoots IG, et al. Cryoablation induces greater inflammatory and coagulative responses than radiofrequency

ablation or laser induced thermotherapy in a rat liver model. *Surgery* 2010; 147:686–695

34. Erinjeri JP, Clark TW. Cryoablation: mechanism of action and devices. *J Vasc Interv Radiol* 2010; 21(8 suppl):S187–S191
35. Dromain C, de Baere T, Elias D, et al. Hepatic tumors treated with percutaneous radio-frequency ablation: CT and MR imaging follow-up. *Radiology* 2002; 223:255–262
36. Lencioni R, Llovet JM. Modified RECIST (mRECIST) assessment for hepatocellular carcinoma. *Semin Liver Dis* 2010; 30:52–60
37. Schraml C, Clasen S, Schwenzer NF, et al. Diagnostic performance of contrast-enhanced computed tomography in the immediate assessment of radiofrequency ablation success in colorectal liver metastases. *Abdom Imaging* 2008; 33:643–651
38. Park Y, Choi D, Rhim H, et al. Central lower attenuating lesion in the ablation zone on immediate follow-up CT after percutaneous radiofrequency ablation for hepatocellular carcinoma: incidence and clinical significance. *Eur J Radiol* 2010; 75:391–396
39. Kim KW, Lee JM, Klotz E, et al. Safety margin assessment after radiofrequency ablation of the liver using registration of preprocedure and postprocedure CT images. *AJR* 2011; 196:[web] W565–W572
40. Fujioka C, Horiguchi J, Ishifuro M, et al. A feasibility study: evaluation of radiofrequency ablation therapy to hepatocellular carcinoma using image registration of preoperative and postoperative CT. *Acad Radiol* 2006; 13:986–994
41. Porter CA, Woodrum DA, Callstrom MR, et al. MRI after technically successful renal cryoablation: early contrast enhancement as a common finding. *AJR* 2010; 194:790–793
42. Goldberg SN, Gazelle GS, Compton CC, Mueller PR, Tanabe KK. Treatment of intrahepatic malignancy with radiofrequency ablation: radiologic-pathologic correlation. *Cancer* 2000; 88:2452–2463